Desalination and Water Treatment
www.deswater.com
doi: 10.5004/dwt.2021.27207

225 (2021) 331–339
June

Red mud reuse for phosphate adsorption via zirconium modification: performance, kinetics, and mechanism

Yan-Long Li, Fakhri Alam, You-Wei Cui*

National Engineering Laboratory for Advanced Municipal Wastewater Treatment and Reuse Technology, Beijing University of Technology, Beijing 100124, China, emails: cyw@bjut.edu.cn (Y.-W. Cui), 18701368656@163.com (Y.-L. Li), fakhrwama@gmail.com (F. Alam)

Received 20 July 2020; Accepted 4 March 2021

ABSTRACT

The reuse of zirconium-modified red mud (Zr-RM) as a phosphate adsorbent for wastewater treatment was assessed herein. The physicochemical properties and phosphate adsorption performance of Zr-RM were investigated, revealing a single-layer adsorption pattern according to the Langmuir isotherm model. The adsorption rate followed a pseudo-second-order model. The maximum phosphate adsorption capacity was 33.14 mg/g and was positively correlated with temperature and initial phosphate concentration, and negatively correlated with the solution pH. In a solution containing fluoride and sulfate ions, due to competitive adsorption, the adsorption capacity of phosphate decreased. The material and wastewater treatment costs of Zr-RM are 0.99 and 61.3 $/kg of P, respectively. This study showed a potential method for using RM with high value for environmental protection.

Keywords: Red mud; Zirconium modification; Phosphate removal; Adsorption; Waste reuse

1. Introduction

Red mud (RM) is a highly alkaline industrial alumina waste product that contains silicon, aluminum, iron, and calcium [1]. Generally, approximately 1.0–1.5 tons of RM waste products are produced per ton of alumina production [2]. The global stock of RM reached nearly 4 billion tons in 2015, with the annual production increasing by approximately 150 million tons [3]. The annual production of RM in China, Australia, India, and Brazil is 88, 30, 10, and 10.6 million tons, respectively [4]. However, due to the very limited use of RM, most of the RM waste is stockpiled on land, seriously endangering environmental safety and human health. The accumulation of RM solids also causes major environmental pollution to surface water, groundwater, soil, and even the atmosphere. The general cost of properly handing RM is US$15 per ton [3], which also increases the financial burden. Therefore, the utilization or recycling of RM resources has become a major issue worldwide.

In order to reduce the accumulation of RM in the environment, attempts were made to reuse RM as construction materials [5], in the extraction of metal elements [6], and as environmental restoration materials [7]. Nevertheless, despite these practices accelerating the reuse of RM, the economic benefits were not substantial. Therefore, the high value-added reuse of RM has become of interest.

Excessive phosphate in water can lead to eutrophication and deterioration of water quality [8]. Therefore, the effluent phosphate discharged from point source treatment facilities is severely restricted. Phosphate removal can be achieved through various techniques, including biological methods [9,10], chemical precipitation [11], electroflocculation [12], adsorption [13,14], and ion exchange [15]. Owing to the simple operation process, the treatment

* Corresponding author.

1944-3994/1944-3986 © 2021 Desalination Publications. All rights reserved.

effectiveness, and the lack of sludge by-products, adsorption technologies have been widely applied for the removal of low-concentration phosphates from wastewater [16]. RM has been shown to absorb phosphorus, fluorine, heavy metals, and some organic matter in wastewater through a simple preparation process (such as acid treatment, heat treatment, and other treatment methods) [17–19]. These discoveries have opened new scenarios for RM reuse as pollution control materials, greatly improving the economic benefits of RM reuse and its importance to the environment. However, Huang et al. [20] modified RM using acid and heat methods to treat phosphate in wastewater and showed that RM has a very low phosphate adsorption capacity (0.58 mg/g). Therefore, the large-scale application of RM as a phosphate adsorbent in the field of wastewater treatment requires effective modification methods to enhance the adsorption capacity of RM.

The adsorption capacity can be enhanced by increasing the specific surface area of RM [21]. ZrO_2 has the potential to increase the specific surface area of inorganic materials and enhances the phosphate surface complexing ability even under acidic and basic conditions [22,23]. Chitrakar et al. [24] synthesized unstructured ZrO_2 by precipitation, demonstrating its high adsorption capacity for phosphate in seawater and synthetic wastewater. These studies indicated that the RM adsorption capacity could be improved through Zr modification. To the best of our knowledge, the modification of RM by Zr to increase its pollutant removal capacity has not been studied to date.

The purpose of this study is to establish the effectiveness and mechanism of Zr modification of RM (Zr-RM) for wastewater treatment. The ability of Zr-RM to remove phosphorus removal was evaluated by establishing the adsorption kinetics and isotherms. The key factors that may affect the adsorption performance were identified to explore the potential application of Zr-RM in wastewater purification.

2. Materials and methods

2.1. Chemicals

The original RM used in the study was collected from a local aluminum corporation, which is the largest aluminum oxide production company in China. RM is an industrial waste product from the Bayer process for aluminum oxide manufacturing. All chemicals and reagents used in the experiment were of analytical grade.

2.2. Preparation of Zr-RM adsorbent

The original RM was first crushed and dried in an oven at 105°C for 48 h. The dried RM was sieved through a 50-mesh grid. The raw chemical of $ZrOCl_2{\cdot}8H_2O$ was also dried to constant weight to remove all crystal water. Subsequently, 7.8241 g of $ZrOCl_2$ and 10 g of RM were mixed with 200 mL of double-distilled water in a beaker to prepare a mixture with a Zr to RM mass ratio of 0.4 as this was shown to have the highest adsorption capacity of materials within a Zr to RM mass ratio range of 0.1–0.5. The mixed liquid-suspended solids were continuously stirred for 3 h for thorough mixing. The pH of the solution was ~7.2. The mixture was then dried at 105°C for 24 h and the powder was crushed, washed, dried, and sieved to 100 mesh as a Zr-RM adsorbent prepared for future use.

2.3. Characterization of Zr-RM adsorbent

The surface morphology of Zr-RM was checked with scanning electron microscopy (SEM; Hitachi, SU8020, Japan). The metallic element composition of Zr-RM was determined by X-ray fluorescence spectrometry (XRF; Shimadzu, XRF-1800, Japan). The specific surface area and pore size distribution of Zr-RM were determined by an adsorption tester (Micromeritics, Gemini V, USA). The X-ray diffraction (XRD) patterns of Zr-RM were detected under Cu Kα radiation of 40 kV and 30 mA and recorded in the range of 2θ from 10° to 70° at a scanning speed range of $0.02°s^{-1}$ (Rigaku, D/max-RB, Japan).

2.4. Batch adsorption experiments

A series of batch experiments of isothermal adsorption, adsorption kinetics, and adsorption conditions were conducted to explore the phosphate adsorption characteristics of the prepared Zr-RM. All batch experiments were carried out in flasks stirred with a magnetic stirrer. The reaction was allowed to proceed for 3 h following preliminary experiments that showed the tested adsorption equilibrium to have been reached by 3 h of reaction. During the experiments, samples were taken regularly. The analysis of phosphorus in the solution was carried out after filtering through a 0.45 μm filter according to the standard method [25]. All batch experiments were performed in triplicate and the average value of the three tests was recorded as the measured value.

In order to study the adsorption isotherms, 50 mg of Zr-RM were placed in 100 mL of phosphate solutions at various initial concentrations (5–100 mg/L) and at a constant temperature of 25°C. The initial pH of the phosphate solution was adjusted to 4 by adding HCl (0.10 M) or NaOH (0.10 M) solution. In the adsorption kinetics test, 0.25 g of the adsorbent were added to a 1,000 mL flask containing 500 mL of the phosphate solution at different concentrations (5, 10, and 30 mg/L) at pH 4. The reaction temperature was constant at 25°C. To establish the key influencing conditions, batch experiments within the range of 5°C–55°C were conducted, where 50 mg of Zr-RM were added to 100 mL of phosphate solution (10 mg/L) at pH 4. The effect of pH (3.0–9.0) of the initial phosphate solution (10 mg/L) was studied at 25°C. Using the same experimental design, through four batches of experiments and using the same concentration of $Cl^-/NO_3^-/F^-/SO_4^{2-}$ in the phosphate solution (10 mg/L), the effect of coexisting anions on phosphate adsorption performance was determined.

2.5. Calculations and simulation

The adsorption capacity of phosphorus on Zr-RM was calculated by Eq. (1). The phosphorus removal efficiency from wastewater was expressed as in Eq. (2). In both formulas, q_e is the amount of phosphate adsorbed in mg/g; C_i and C_e are the

initial and final phosphate concentrations in mg/L; V is the volume of phosphate in L; and M is the mass of Zr-RM in g.

$$q_e = \frac{\left(C_i - C_e\right)}{M} \times V \tag{1}$$

The Langmuir [Eq. (2)] and Freundlich [Eq. (3)] isotherms were used to establish the adsorption models [13,26]:

$$\frac{C_e}{q_e} = \frac{1}{K_L q_m} + \frac{C_e}{q_m} \tag{2}$$

$$\log q_e = \log K_F + \frac{1}{n}\log C_e \tag{3}$$

where C_e is the concentration of the phosphate solution at equilibrium (mg/L); q_e is the corresponding adsorption capacity (mg/g); K_L is the constant of the Langmuir model related to the free energy of adsorption (L/mg); q_m is the single-layer adsorption capacity of Zr-RM (mg/g); K_F is the constant of the Freundlich model (L/g); and n is the heterogeneity factor of the adsorbent related to the adsorption process.

Pseudo-first-order [Eq. (4)] and pseudo-second-order [Eq. (5)] models were used to calculate the reaction kinetics [27,28]:

$$\log\left(q_e - q_t\right) = \log q_e - \frac{k_1 t}{2.303} \tag{4}$$

$$\frac{t}{q_t} = \frac{1}{k_2 q_e^2} + \frac{t}{q_e} \tag{5}$$

where q_e and q_t are the amount of phosphate adsorbed on Zr-RM at equilibrium, over a given time, in mg/g; t is the contact time in min; k_1 is the pseudo-first-order adsorption model parameter in L/min; k_2 is the pseudo-second-order kinetic model parameter in g/(mg min); and h is the initial rate coefficient, equal to $k_2 q_e^2$ in mg/(g min).

The Gibbs free energy ($\Delta G°$), enthalpy ($\Delta H°$), and entropy ($\Delta S°$) were calculated to evaluate the thermodynamics of the adsorption process, using Eqs. (6)–(8) [17]:

$$\Delta G° = -RT\ln K \tag{6}$$

$$\Delta G° = \Delta H° - T\Delta S° \tag{7}$$

$$K = \frac{aq_e}{C_e} \tag{8}$$

where R and T are the universal gas constant (8.314 J/mol K) and temperature (K); K is the equilibrium constant; and a is the adsorbent dose (g/L).

3. Results and discussion

3.1. Adsorption isotherm

The adsorption isotherm curve of Zr-RM at 25°C is shown in Fig. 1. As the initial concentration of phosphate

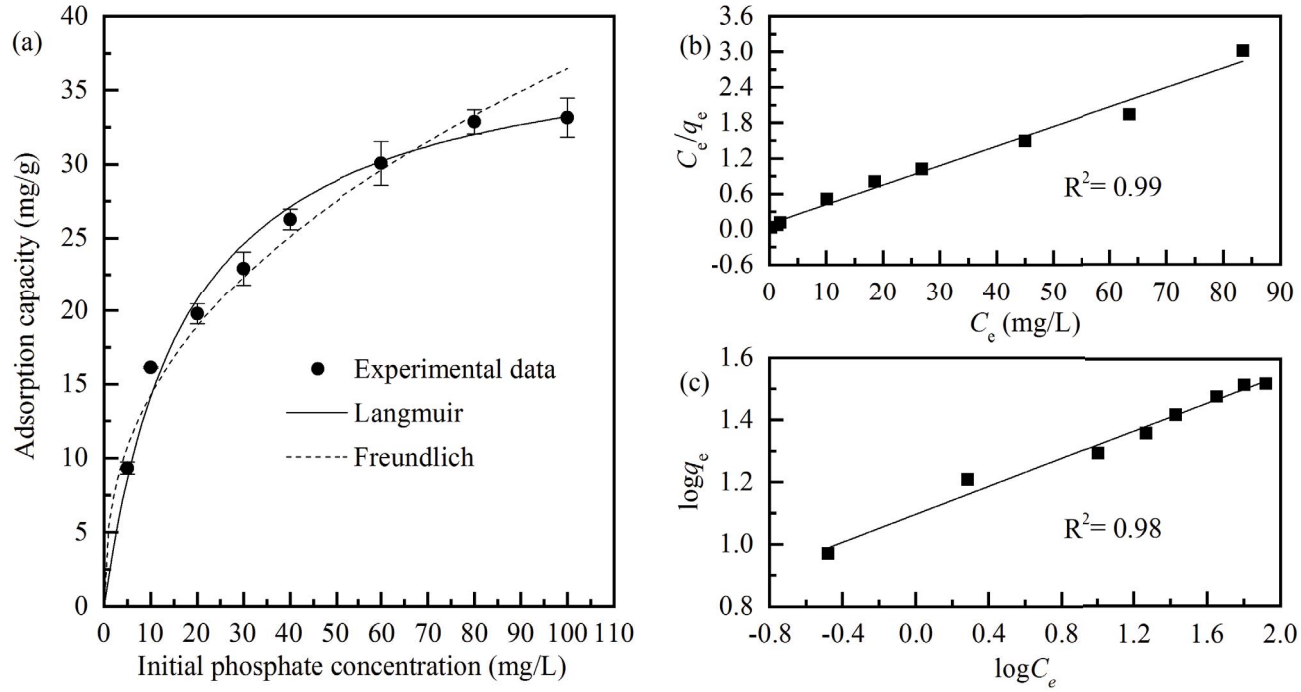

Fig. 1. Experimental and theoretical adsorption isotherm of phosphate on Zr-RM (dosage 0.5 g/L, temperature 25°C, solution pH 4, adsorption time 3 h). (a) Isotherms of phosphate on Zr-RM. Fitting calculation curve by (b) Langmuir isotherm model and (c) Freundlich isotherm model. The measured data are indicated by (■), Langmuir isotherm model fitting is indicated by (——), and Freundlich isotherm model fitting is indicated by (- - - -).

in the solution increased, the adsorption capacity also increased. When the initial concentration of phosphate increased from 80 to 100 mg/L, a very small increasing trend was noticed, indicating that the maximum adsorption capacity was close to 33.14 mg/g. The Langmuir isotherm model and Freundlich isotherm model adequately described the equilibrium adsorption data (Figs. 1b and c). The calculated maximum theoretical saturation adsorption capacity was 34.86 mg/g. The Langmuir isotherm suggests that the adsorption of phosphorus by Zr-RM occurs as a monolayer surface chemical adsorption. Thus, theoretically, the adsorbed particles are independent of each other and the interaction between the adsorbed particles is negligible. Therefore, the maximum adsorption capacity of Zr-RM depends on the adsorption site. According to the Freundlich isotherm, the reciprocal of the heterogeneity factor (n) is 0.4, indicating that adsorption is prone to occur and that the effect of the pollutant concentration is very small. Some adsorbents that use Zr as a modifying agent exhibit similar adsorption characteristics as Zr-RM (Table 1) [29–31]. The use of Zr as a modifying agent may lead to a high adsorption capacity due to the increase in the number of adsorption sites. In contrast, the maximum saturation adsorption capacity of Zr-RM is lower than that of Zr-modified single compounds, such as Zr-based metal-organic frameworks and Zr-cross-linked N-2-hydroxypropyl trimethyl ammonium chloride chitosan/bentonite, likely due to the fact that RM is a mixture containing various metallic and non-metallic compounds (Table 1), thereby reducing the effective adsorption site per unit mass. RM is usually acidified to absorb phosphorus. Compared with acid-modified RM [20], the adsorption capacity of Zr-RM was more than 75 times greater (Table 2), indicating that Zr plays an important role in improving the adsorption capacity of phosphorus.

3.2. Adsorption kinetics and thermodynamics

In order to understand the adsorption process, pseudo-first-order and pseudo-second-order kinetic models were used (Fig. 2). For the pseudo-second-order model, the correlation coefficient (R^2) was greater than 0.98, regardless of the initial phosphorus concentration, indicating that the adsorption behavior follows a pseudo-second-order

Table 1
Metallic element composition of RM and Zr-RM

	RM/wt.%	Zr-RM/wt.%
Si	9.29	5.89
Ti	2.56	1.56
Ca	11.47	0.63
Al	11.60	7.04
Cl	0.011	1.46
Fe	8.68	5.33
K	1.57	0.61
Mg	0.61	0.36
Na	5.30	0.1
Zr	0.13	26.58

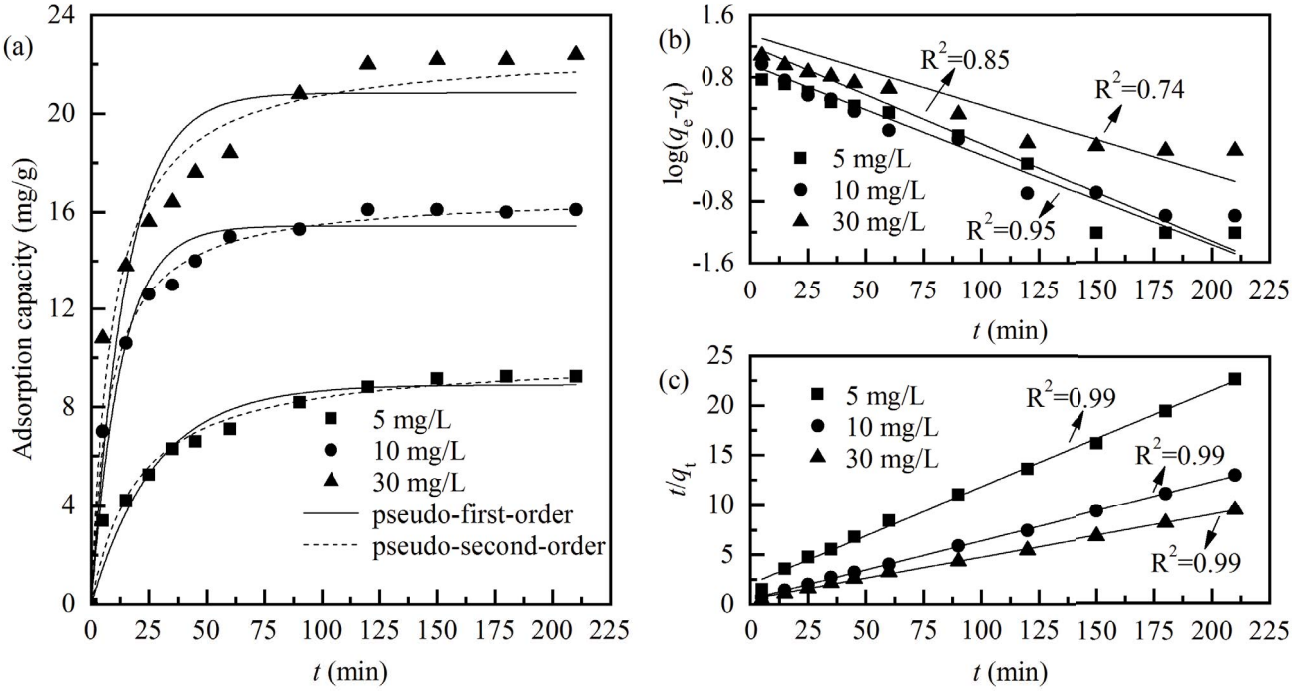

Fig. 2. Experimental and theoretical adsorption kinetics of phosphate on Zr-RM (adsorbent dosage 0.5 g/L, temperature 25°C, solution pH 4, initial phosphate concentration 10 mg/L). (a) Kinetics of phosphate adsorption on Zr-RM, (b) pseudo-first-order, (c) pseudo-second-order kinetics fitting calculation curve. The measured data at 5 mg/L (■), 10 mg/L (●), and 30 mg/L (▲) are shown. The pseudo-first-order kinetics fitting is indicated by (——) and pseudo-second-order kinetics fitting is indicated by (- - - - -).

Table 2
Comparison of absorption characteristics with the modification adsorbents for phosphorus removal

Adsorbent	Langmuir			Freundlich			Reference
	q_m	K_L	R^2	n	K_f	R^2	
Zr-based MOFs frameworks	167	0.046	0.99	1.98	16.52	0.98	[29]
Fe–Zr binary oxide	24.91	7.07	0.85	11.72	19.26	0.54	[30]
Zr-Crosslinked HACC/BT	65.35	0.094	0.99	3.33	14.55	0.99	[31]
Acid-modified RM	0.46	146.39	0.91	4.28	0.62	0.91	[20]
Zr-RM	34.86	0.064	0.99	2.46	5.59	0.96	This work

kinetic model. In general, the adsorption kinetics can be controlled by the reaction rate, mass transfer, and pore filling of porous adsorbents. The pseudo-second-order behavior indicated that Zr-RM phosphate adsorption may be caused by chemical adsorption [32], consistent with the results of the adsorption isotherms. Therefore, a chemical reaction rather than the mass transfer step is the rate-limiting step of adsorption. According to thermodynamic calculations, the adsorption reaction can occur spontaneously (Table 3). The adsorption process of some absorbents modified by Zr and RM adsorbents also followed the pseudo-second-order model (Table 3). The Zr-modified adsorbent has a higher h value, indicating that the adsorption rate is higher in the initial stage of the reaction. In contrast, the h value of Zr-RM is only one-tenth or less than that of other modified materials and is nearly 100 times higher than that of acid-modified RM. Thus, Zr modification can significantly improve the adsorption rate of RM.

3.3. Key influencing factors

The high adsorption capacity of Zr-RM was observed in acidic solution. As the pH of the solution increased, the phosphate adsorption capacity of Zr-RM gradually decreased (Fig. 3a). At the pH range of 3–7, the pH value of the solution played a major role on the adsorption capacity of Zr-RM. Compared with the adsorption capacity at pH 3, at pH 7, the adsorption capacity was reduced two-fold. At a pH above 7, the effect of pH on the adsorption capacity became very small, likely due to the chemical reaction of Zr-RM in different pH solutions. The hydration process of the main elements in Zr-RM (such as aluminum and zirconium) depends on the pH of the solution, which is the key to chemical adsorption. In addition, since the surface of RM may be more negatively charged in a solution with an increased pH, the decrease in Zr-RM adsorption capacity may be due to the increase in repulsion of phosphate species by the negative charges [33]. Finally, at different pH solutions, the existence of phosphate ions in water is also different. At a pH value lower than 7.2, the phosphate is mainly present in the form of $H_2PO_4^-$, whereas at pH 7.2–12.3 phosphate is present as HPO_4^{2-} [34]. Owing to the difference in electronegativity between $H_2PO_4^-$ and HPO_4^{2-} anions, the reaction of phosphate anions with Zr-RM could thus differ.

The influence of temperature on phosphate absorption was also assessed. In the test range of 5°C–55°C, the adsorption capacity of phosphate increased with increasing reaction temperature (Fig. 3b). These results indicated that the adsorption reaction is endothermic, which is consistent with thermodynamics (Table 3). Temperature plays a positive role in improving the adsorption capacity of phosphate.

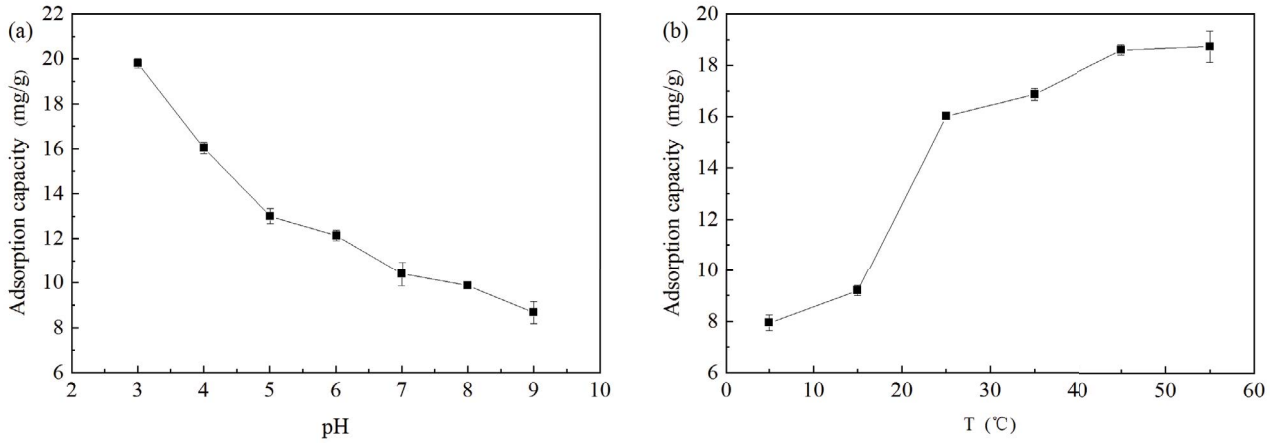

Fig. 3. (a) Effect of pH on the phosphate adsorption capacity of Zr-RM (adsorbent dosage 0.5 g/L, reaction temperature 25°C, initial phosphate concentration 10 mg/L, reaction time 3 h). (b) Effect of temperature on the phosphate adsorption capacity of Zr-RM (adsorbent dosage 0.5 g/L, solution pH 4, initial phosphate concentration 10 mg/L, reaction time 3 h). The measured data are indicated by (■).

Table 3
Pseudo-second-order kinetics and thermodynamics parameters

Adsorbent	Pseudo-second-order kinetics			Thermodynamics			Reference
	h	k_2	R^2	$\Delta G°$	$\Delta H°$	$\Delta S°$	
Zr-based MOFs frameworks	13.9	0.0068	0.975	–	–	–	[29]
Fe–Zr binary oxide	26.4	0.05	0.953	–	–	–	[30]
Zr-Crosslinked HACC/BT	90.2	0.913	1	–19.4	–13.3	0.112	[31]
Acid-modified RM	0.02	0.0718	0.99	–	–	–	[20]
Zr-RM	1.9	0.0036	0.99	–3.46	52.107	0.1832	This work

"–" means that data is not available.

When the reaction occurs above 25°C, the increase in adsorption capacity is not obvious; thus, considering the economic factors, this may be the optimal temperature for practical engineering.

The co-existing anions may compete for the phosphate adsorption sites of Zr-RM. At an initial phosphate concentration of 10 mg/L, the effects of various coexisting anions (F^-, SO_4^{2-}, NO_3^-, and Cl^-) on phosphate adsorption were investigated (Fig. 4). In the solution containing Cl^- or NO_3^- co-existing anions, the adsorption capacity of phosphate remained constant, while in the solution containing F^- or SO_4^{2-} coexisting anions, the adsorption capacity of phosphate was significantly reduced. Competitive adsorption usually occurred in anions with similar chemisorption characteristics, indicating that the co-existing anion of F^- or SO_4^{2-} can follow a similar chemical adsorption reaction for phosphate. In future engineering design, the effects caused by competitive adsorption should be fully considered for real wastewater samples.

3.4. Adsorption mechanism

The SEM images of RM and Zr-RM before and after phosphate adsorption were obtained (Fig. 5). The surface of the original RM particles was relatively smooth (Fig. 5a). After modification with Zr, convex particles attached to the Zr-RM surface were observed (Fig. 5b), indicating the formation of Zr compounds. After phosphate adsorption, the surface of Zr-RM became rough with irregularly shaped layered deposits (Fig. 5c). After modification, the specific surface area of Zr-RM was significantly increased by 11 times compared with the original RM (Table 4). The increase in specific surface area may be due to the decrease in average pore size. The average pore size of Zr-RM was nine-fold lower than the original RM. It has been previously reported that compound

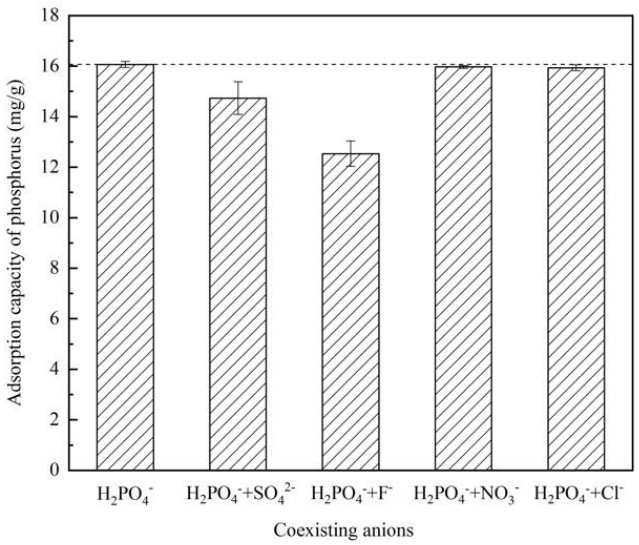

Fig. 4. Effect of coexisting anions on phosphate uptake by Zr-RM (adsorbent dosage 0.5 g/L, reaction temperature 25°C, initial phosphate concentration 10 mg/L, solution pH 4, reaction time 3 h). The line (- - - -) shows the adsorption capacity of Zr-RM in solution without coexisting ions.

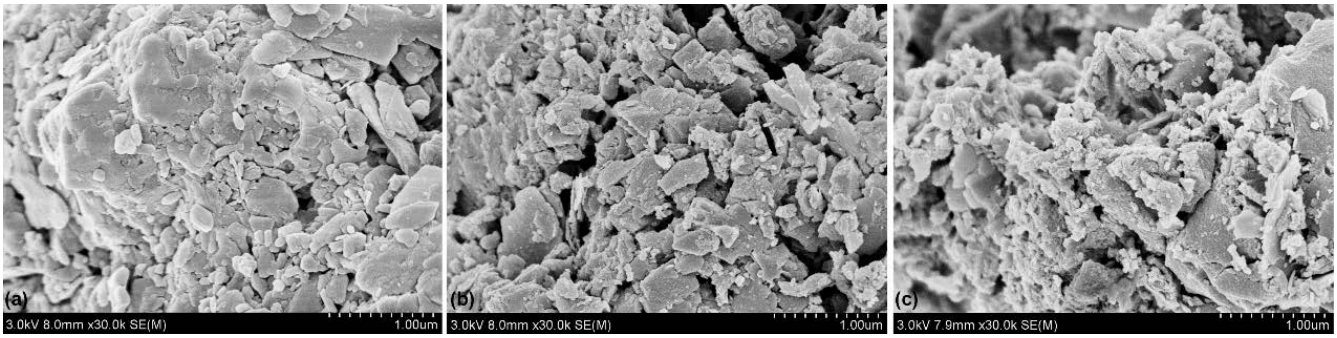

Fig. 5. SEM image of (a) RM, (b) Zr-RM, and (c) Zr-RM with adsorbed phosphate.

Table 4
Pore properties of RM and Zr-RM

	Specific surface area (m^2/g)	Pore volume (cm^3/g)	Average pore radius (nm)
RM frameworks	7.77	0.056	28.73
Zr-RM	96.97	0.076	3.13

crystals can be formed after acid modification, resulting in an increase in RM specific surface area ranging from 14.09 to 19.35 m^2/g [35]. From the significant increase in specific surface area after Zr element modification, it can be inferred that the convex particles adhered onto Zr-RM play a key role in adsorption. Furthermore, Zr increased the specific surface area of the material, thus accounting for the greater adsorption capacity of Zr-RM than of RM.

The Langmuir isotherm indicated that the Zr-RM adsorption chemistry of phosphate occurred on the surface of the adsorbent. In order to determine a possible reaction, the crystal composition was established using XRD (Fig. 6). According to the standard JCPDS card and the diffraction peaks of ferric oxide appearing in the RM diffraction pattern, the main phases of crude RM were determined to be katoite, kaolinite, and cancrinite. The results can be further verified by the elemental composition of crude RM (Table 1). The chemical elements that form these compounds, for example, Al, Ca, Si, and Na, were observed to be abundant in the raw RM. In a neutral aqueous solution, these crude RM crystals cannot react with phosphate due to their low solubility, which explains the negligible phosphate adsorption on crude RM. Even following acid modification, these crude crystals, such as katoite, kaolinite, and cancrinite, showed a very low phosphate adsorption capacity (0.58 mg/g) due to their low reactivity with phosphate [20].

Following modification with the Zr element, two diffraction patterns were observed. One of the main phases of Zr-RM was tetragonal $Al(OH)_3$. Owing to the high content of Al, tetragonal $Al(OH)_3$ is easily formed during the acidification and activation of aluminum oxides (Table 4). Although Zr was the main element, accounting for 26.58% of the weight content in Zr-RM (Table 1), the XRD analysis did not show any crystals containing Zr elements (Fig. 6). Therefore, it is reasonable to deduce that Zr would be the amorphous form in Zr-RM. According to a previous report [24], the taro peak that was formed between the diffraction angles of 20° and 35° was the amorphous $Zr(OH)_4$ (Fig. 6). Therefore, the other main phase was determined as amorphous $Zr(OH)_4$. Amorphous $Zr(OH)_4$ not only greatly increased the specific surface area but also adsorbed phosphate on Zr-RM through ion exchange between hydroxyl and phosphate [26,36]. The reaction of $Al(OH)_3$ with phosphate was also confirmed by observing that the intensity of the $Al(OH)_3$ diffraction peak was considerably reduced following phosphate adsorption (Fig. 6). Therefore, it can be concluded that the adsorption of Zr-RM is mainly caused by the chemical reaction of $Al(OH)_3$ and amorphous $Zr(OH)_4$ with phosphate. Theoretically, these two reactions occur through an ion exchange reaction between the hydroxyl group and phosphate in solution [17]. Since the phosphate forms differed according to the pH of the solution, the reaction could be expressed by Eqs. (9)–(12):

$$\equiv Al-OH+H_2PO_4^- \leftrightharpoons \equiv AlH_2PO_4+OH^- \quad (2.1<pH<7.2) \tag{9}$$

$$2\equiv Al-OH+HPO_4^{2-} \leftrightharpoons (\equiv Al)_2HPO_4+2OH^- \quad (7.2<pH<12.3) \tag{10}$$

$$\equiv Zr-OH+H_2PO_4^- \leftrightharpoons \equiv Zr-OPO_3H_2+OH^- \quad (2.1<pH<7.2) \tag{11}$$

$$\equiv Zr-OH+HPO_4^{2-} \leftrightharpoons Zr-OPO_3H^-+OH^- \quad (7.2<pH<12.3) \tag{12}$$

3.5. Economic analysis

According to the above, the phosphate adsorption capacity of Zr-RM is affected by the initial phosphate concentration, reaction solution pH, and reaction time. If a sufficient dosage of adsorbent was provided (the total adsorption capacity of the used adsorbent was more than the total amount of phosphorus in water), the effluent phosphate concentration was lower than 0.2 mg/L independent of initial phosphate concentration when the adsorption reached equilibrium. Therefore, the application of Zr-RM showed the technical appeal for enhanced phosphorus

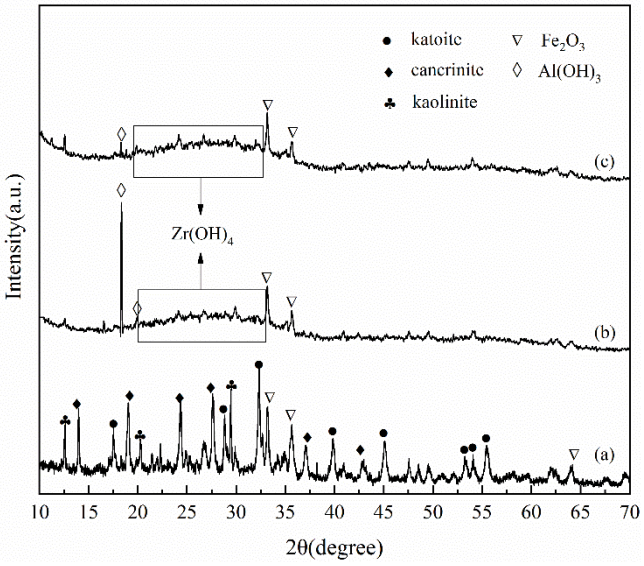

Fig. 6. Powder XRD pattern of RM (line a), Zr-RM (line b), and Zr-RM after adsorption of phosphate (line c). The different phases are shown: katoite (●), cancrinite (◆), kaolinite (♣), Fe_2O_3 (▽), and $Al(OH)_3$ (◇).

removal from wastewater treatment. Besides the technological advantages, the economics of the adsorbents could be viewed as the important factor influencing the further application of Zr-RM. The economics of the adsorbents are dependent on the chemical costs as well as the costs related to the manufacture. Since the cost of RM is very low, the material cost of Zr-RM is of ~0.99 $/kg, which can be ranked as a low-cost adsorbent [37]. Herein, the phosphorus concentration (10 mg/L) was simulated according to that present in common municipal wastewater. When the prepared Zr-RM was used to treat this kind of wastewater, the treatment cost was estimated at 61.3 $/kg P, which is lower than that of porous metal oxides and hybrid ion exchange resins (~100 $/kg P) and than that of a chemical precipitation method (~70 $/kg P) [37]. The cost of Zr-RM could be further reduced by replenishing the adsorbent active sites. The adsorbent cost is reported as a function of both regeneration cycles and the regeneration cost [37]. In view of the adsorption reaction of amorphous $Zr(OH)_4$ with phosphate, strong alkali chemicals could be used in the generation of Zr-RM. In this situation, due to the higher cost of alkali chemicals than that of RM, and even that of Zr-RM, the further lowering the economics of Zr-RM adsorbent by means of generation could show the low sensitivity.

4. Conclusions

This study was conducted to determine the feasibility of RM reuse for phosphate adsorption via Zr modification. RM was re-used as a raw material to prepare phosphate adsorbents through Zr modification, providing a potential solution to the accumulation of RM waste in the environment. Adsorption experiments showed that Zr-RM has a strong phosphate adsorption performance and a high phosphate adsorption capacity of 33.14 mg/g, which was positively related to the reaction temperature and the initial phosphate concentration in the solution but negatively related to the pH of the solution. Owing to competitive adsorption, the presence of F^- and SO_4^{2-} in the phosphate solution reduced the phosphate adsorption capacity. Following the Langmuir isotherm model and pseudo-second-order kinetic model, the adsorption of phosphate on Zr-RM is a single layer ion-exchange reaction between $Al(OH)_3$ and amorphous $Zr(OH)_4$ and phosphate. Following Zr modification, the specific surface area of RM increased to 96.97 m^2/g, providing a large number of adsorption sites. The material and treatment costs of Zr-RM are 0.99 and 61.3 $/kg P, respectively, showing high economic and environmental benefits.

Acknowledgments

This study was supported by the National Natural Science Foundation of China (Project No. 51878010) and Great Wall Scholar Program of the Beijing Municipal High-level Faculty (CIT&TCD20190310).

References

[1] S. Aydin, M.E. Aydin, F. Beduk, B. Fatma, U. Arzu, Removal of antibiotics from aqueous solution by using magnetic Fe_3O_4/red mud-nanoparticles, Sci. Total Environ., 670 (2019) 539–546.

[2] F. Ni, J.S. He, Y.B. Wang, Z.K. Luan, Preparation and characterization of a cost-effective red mud/polyaluminum chloride composite coagulant for enhanced phosphate removal from aqueous solutions, J. Water Process Eng., 6 (2015) 158–165.

[3] L. Wang, N. Sun, H.H. Tang, W. Sun, A review on comprehensive utilization of red mud and prospect analysis, Minerals, 9 (2019) 362, doi: 10.3390/min9060362.

[4] E. Mukiza, L.L. Zhang, X. Liu, N. Zhang, Utilization of red mud in road base and subgrade materials: a review, Resour. Conserv. Recyl., 141 (2019) 187–199.

[5] P. Krivenko, O. Kovalchuk, A. Pasko, T. Croymans, M. Hult, G. Luttee, N. Vandevenne, S. Schreurs, W. Schroeyers, Development of alkali activated cements and concrete mixture design with high volumes of red mud, Constr. Build. Mater., 6 (2017) 819–826.

[6] C.L. Liu, S.H. Ma, S.L. Zheng, Y. Luo, J. Ding, X.H. Wang, Y. Zhang, Combined treatment of red mud and coal fly ash by a hydro-chemical process, Hydrometallurgy, 175 (2018) 224–231.

[7] P. Hu, Y.H. Zhang, F.Z. Lv, W.S. Tong, H. Xin, Z.L. Meng, X.K. Wang, P.K. Chu, Preparation of layered double hydroxides using boron mud and red mud industrial wastes and adsorption mechanism to phosphate, Water Environ. J., 31 (2017) 145–157.

[8] B.H. Thagira, P. Karthikeyan, S. Meenakshi, Lanthanum(III) encapsulated chitosan-montmorillonite composite for the adsorptive removal of phosphate ions from aqueous solution, Int. J. Biol. Macromol., 112 (2018) 284–293.

[9] C. Tarayre, R. Charlier, A. Delepierre, A. Brognaux, J. Bauwens, F. Francis, M. Dermience, G. Logany, B. Taminiau, G. Daube, P. Compere, E. Meers, E. Michels, F. Delvigne, Looking for phosphate-accumulating bacteria in activated sludge processes: a multidisciplinary approach, Environ. Sci. Pollut. Res., 24 (2017) 8017–8032.

[10] D. Yadav, V. Pruthi, P. Kumar, Enhanced biological phosphorus removal in aerated stirred tank reactor using aerobic bacterial consortium, J. Water Process Eng., 13 (2016) 61–69.

[11] A.H. Caravelli, G.C. De, N.E. Zaritzky, Effect of operating conditions on the chemical phosphorus removal using ferric chloride by evaluating orthophosphate precipitation and sedimentation of formed precipitates in batch and continuous systems, Chem. Eng. J., 209 (2012) 469–477.

[12] P.I. Omwene, M. Kobya, Treatment of domestic wastewater phosphate by electrocoagulation using Fe and Al electrodes: a comparative study, Process Saf. Environ. Prot., 116 (2018) 34–51.

[13] S.M. Ding, Q. Sun, X. Chen, Q. Liu, D. Wang, J. Lin, C.S. Zhang, D.C.W. Tsang, Synergistic adsorption of phosphorus by iron in lanthanum modified bentonite (Phoslock®): new insight into sediment phosphorus immobilization, Water Res., 134 (2018) 32–43.

[14] B.Q. Zhang, N. Chen, C.P. Feng, Z.Y. Zhang, Adsorption for phosphate by crosslinked/non-crosslinked-Chitosan-Fe(III) complex sorbents: characteristic and mechanism, Chem. Eng. J., 353 (2018) 361–372.

[15] C.J. Paul, M. Chua, B. Zhang, Effects of competitive ions, humic acid, and pH on removal of ammonium and phosphorous from the synthetic industrial effluent by ion exchange resins, Waste Manage., 22 (2002) 711–719.

[16] W.P. Xiong, J. Tong, Z.H. Yang, G.M. Zeng, Y.Y. Zhou, D.B. Wang, P.P. Song, R. Xu, C. Zhang, M. Cheng, Adsorption of phosphate from aqueous solution using iron-zirconium modified activated carbon nanofiber: performance and mechanism, J. Colloid Interface Sci., 493 (2017) 17–23.

[17] J. Ye, X.N. Cong, P.Y. Zhang, E. Hoffmann, G.M. Zeng, Y. Liu, W. Fang, Y. Wu, H.B. Zhang, Interaction between phosphate and acid-activated neutralized red mud during adsorption process, Appl. Surf. Sci., 356 (2015) 128–134.

[18] Y.W. Cui, J. Li, Z.F. Du, Y.Z. Peng, Cr(VI) adsorption on red mud modified by lanthanum: performance, kinetics and mechanisms, PLoS One, 11 (2016) e0161780, doi: 10.1371/journal.pone.0161780.

[19] A. Bhatnagar, V.J.P. Vilar, C.M.S. Botelho, R.A.R. Boaventura, A review of the use of red mud as adsorbent for the removal of toxic pollutants from water and wastewater, Environ. Technol., 32 (2011) 231–249.
[20] W.W. Huang, S.B. Wang, Z.H. Zhu, L. Li, X.D. Yao, V. Rudolph, F. Haghseresht, Phosphate removal from wastewater using red mud, J. Hazard. Mater., 158 (2008) 35–42.
[21] G.F. Hulya, C.T.D. Jens, D. Mcconchie, Increasing the arsenate adsorption capacity of neutralized red mud (Bauxsol), J. Colloid Interface Sci., 271 (2004) 313–320.
[22] Y. Su, H. Cui, Q. Li, S. Gao, J.K. Shang, Strong adsorption of phosphate by amorphous zirconium oxide nanoparticles, Water Res., 47 (2013) 5018–5026.
[23] N. Pitakteeratham, A. Hafuka, H. Satoh, Y. Watanabe, High efficiency removal of phosphate from water by zirconium sulfate-surfactant micelle mesostructure immobilized on polymer matrix, Water Res., 47 (2013) 3583–3590.
[24] R. Chitrakar, S. Tezuka, A. Sonoda, K. Sakane, K. Ooi, T. Hirotsu, Selective adsorption of phosphate from seawater and wastewater by amorphous zirconium hydroxide, J. Colloid Interface Sci., 297 (2006) 426–433.
[25] APHA, Standard Methods for the Examination of Water and Wastewater, American Public Health Association, USA, 1995.
[26] Y.H. Zhan, H.H. Zhang, J.W. Lin, Z. Zhang, J. Gao, Role of zeolite's exchangeable cations in phosphate adsorption onto zirconium-modified zeolite, J. Mol. Liq., 243 (2017) 624–637.
[27] M. Borandegi, A. Nezamzadeh-Ejhieh, Enhanced removal efficiency of clinoptilolite nano-particles toward Co(II) from aqueous solution by modification with glutamic acid, Colloid Surf., A, 479 (2015) 35–45.
[28] Y.H. He, H. Lin, Y.B. Dong, L. Wang, Preferable adsorption of phosphate using lanthanum-incorporated porous zeolite: characteristics and mechanism, Appl. Surf. Sci., 426 (2017) 995–1004.
[29] K.Y.A. Lin, S.Y. Chen, A.P. Jochems, Zirconium-based metal organic frameworks: highly selective adsorbents for removal of phosphate from water and urine, Mater. Chem. Phys., 160 (2015) 168–176.
[30] Z.M. Ren, L.N. Shao, G.S. Zhang, Adsorption of phosphate from aqueous solution using an iron–zirconium binary oxide sorbent, Water Air Soil Pollut., 223 (2012) 4221–4231.
[31] J. Wang, Y.P. Liu, P. Hu, R.H. Huang, Adsorption of phosphate from aqueous solution by Zr(IV)-crosslinked quaternized chitosan/bentonite composite, Environ. Prog. Sustainable Energy, 37 (2018) 267–275.
[32] J. Lalley, C. Han, X. Li, D.D. Dionysiou, N.M. Nadagouda, Phosphate adsorption using modified iron oxide-based sorbents in lake water: kinetics, equilibrium, and column tests, Chem. Eng. J., 284 (2016) 1386–1396.
[33] V.M. Tangde, S.S. Prajapati, B.B. Mandal, N.P. Kulkarni, Study of kinetics and thermodynamics of removal of phosphate from aqueous solution using activated red mud, Int. J. Environ. Res., 11 (2017) 39–47.
[34] J. Goscianska, M. Ptaszkowska-Koniarz, M. Frankowski, R. Panek, W. Franus, Removal of phosphate from water by lanthanum-modified zeolites obtained from fly ash, J. Colloid Interface Sci., 513 (2018) 72–81.
[35] Y.Z. Li, C.J. Liu, Z.K. Luan, X.J. Peng, C.L. Zhu, Z.Y. Chen, Z.G. Zhang, J.H. Fan, Z.P. Jia, Phosphate removal from aqueous solutions using raw and activated red mud and fly ash, J. Hazard. Mater., 137 (2006) 374–383.
[36] T.S.S. Freire, M.W. Clark, M.J. Comarmond, T.E. Payne, A.J. Reichelt-Brushett, G.J. Thorogood, Electroacoustic isoelectric point determinations of bauxite refinery residues: different neutralisation techniques and minor mineral effects, Langmuir, 28 (2012) 11802–11811.
[37] P.S. Kumar, L. Korving, M.C.M. Loosdrecht, G.J. Witkamp, Adsorption as a technology to achieve ultra-low concentrations of phosphate: research gaps and economic analysis, Water Res., 4 (2019) 100029, doi: 10.1016/j.wroa.2019.100029.